6-1-2012

A Parametric Study of the Low-Impulse Blast Behaviour of Fibre-Metal Laminates Based on Different Aluminium Alloys

Thuc Vo
Glyndwr University, t.vo@glyndwr.ac.uk

Zhongwei Guan
University of Liverpool

Wesley Cantwell
University of Liverpool

Graham Schleyer
University of Liverpool

A Parametric Study of the Low-Impulse Blast Behaviour of Fibre-Metal Laminates Based on Different Aluminium Alloys

Abstract
A parametric study has been undertaken in order to investigate the influence of the properties of the aluminium alloy on the blast response of fibre-metal laminates (FMLs). The finite element (FE) models have been developed and validated using experi-mental data from tests on FMLs based on a 2024-O aluminium alloy and a woven glass-fibre/polypropylene composite (GFPP). A vectorized user material subroutine (VUMAT) was employed to define Hashin's 3D rate-dependant damage constitutive model of the GFPP. Using the validated models, a parametric study has been carried out to investigate the blast resistance of FML panels based on the four aluminium alloys, namely 2024-O, 2024-T3, 6061-T6 and 7075-T6. It has been shown that there is an approximation linear relationship between the dimensionless back face displacement and the dimensionless impulse for all aluminium alloys investigated here. It has also shown that the residual displacement of back surface of the FML panels and the internal debonding are dependent on the yield strength of the aluminium alloy.

Keywords
Fibre-metal laminates, Localised blast loading, Hashin's 3D failure criteria, Strain-rate effects, Finite element models

Disciplines
Aerospace Engineering | Mechanical Engineering

A Parametric Study of the Low-Impulse Blast Behaviour of Fibre-Metal Laminates Based on Different Aluminium Alloys

Thuc Vo[1], Zhongwei Guan[2], Wesley Cantwell[2], Graham Schleyer[2]

[1] School of Mechanical, Aeronautical and Electrical Engineering, Glyndŵr University, Plas Coch, Mold Road, Wrexham, LL11 2AW, UK
[2] School of Engineering, University of Liverpool, Brownlow Street, Liverpool, L69 3GQ, UK

Abstract: A parametric study has been undertaken in order to investigate the influence of the properties of the aluminium alloy on the blast response of fibre-metal laminates (FMLs). The finite element (FE) models have been developed and validated using experimental data from tests on FMLs based on a 2024-O aluminium alloy and a woven glass-fibre/polypropylene composite (GFPP). A vectorized user material subroutine (VUMAT) was employed to define Hashin's 3D rate-dependant damage constitutive model of the GFPP. Using the validated models, a parametric study has been carried out to investigate the blast resistance of FML panels based on the four aluminium alloys, namely 2024-O, 2024-T3, 6061-T6 and 7075-T6. It has been shown that there is an approximation linear relationship between the dimensionless back face displacement and the dimensionless impulse for all aluminium alloys investigated here. It has also shown that the residual displacement of back surface of the FML panels and the internal debonding are dependent on the yield strength of the aluminium alloy.

Key Words: Fibre-metal laminates, Localised blast loading, Hashin's 3D failure criteria, Strain-rate effects, Finite element models.

1. Introduction

Fibre-metal laminates (FMLs) are hybridised metal and composite structural materials that have been attracting interest from a number of researchers due to their improved fatigue and impact resistance (Vlot, 1996; Krishnakumar, 1994; Vogelesang and Vlot, 2000; Compston et al., 2001; Reyes-Villanueva and Cantwell, 2004; Reyes and Cantwell, 2000). The most commonly used FML is GLARE, which comprises thin aluminium 2024-T3 sheets and a unidirectional or a biaxial glass-fibre-reinforced epoxy. The blast response of FMLs has received attention in a number of experimental studies. Fleischer (1996) presented data from blast test results on a lightweight luggage container based on GLARE and reported that it was capable of withstanding a bomb blast greater than that in the Lockerbie air disaster. Langdon et al. (2007a, 2007b) and Lemanski et al. (2007) carried out blast tests of FML panels based on a 2024-O aluminium alloy and a glass fibre reinforced polypropylene. Blast tests on FML panels based on other composites, such as a glass fibre polyamide matrix and GLARE were also been undertaken by Langdon et al. (2007c, 2009). Since experimental trials are usually very costly and time-consuming, it is evident that modelling the blast behaviour of FMLs using commercial finite element software would be great interest. Once these models are verified, they can be used to predict the response of FMLs based on different configurations, lay-ups, loading and boundary conditions without the need to undertake a large number of experimental tests. However, in spite of the fact that there have been a number of experimental studies on the blast behaviour of FMLs, relatively little work has been conducted to model their response. Kotzakolios et al. (2011a) used LS-DYNA to investigate the blast response of GLARE laminates-comparison against experimental results. Later, Kotzakolios et al. (2011b) extended their research to investigate the damage induced in a typical commercial fuselage based on aluminium and GLARE, when subjected to an explosive charge. Soutis et al. (2011) investigated the structural response of fully clamped GLARE panels to blast loads using LS-DYNA. Karagiozova et al. (2010) modelled the blast response of FML panels based on various stacking configurations using ABAQUS/Explicit in order to predict the influence of the loading parameters and structural characteristics on their overall behaviour. However, damage occurring inside the composite material was not considered in the analysis.

In this paper, rate-dependent failure criteria for a unidirectional composite are developed by modifying Hashin's 3D failure criteria (Hashin, 1980). The constitutive model and failure criteria are then implemented in ABAQUS/Explicit using the VUMAT subroutine. The FE models were developed and validated using experimental data from tests on FMLs based on a 2024-O aluminium alloy and a woven glass-fibre/polypropylene composite. Using the validated models, a parametric study was carried out to investigate the influence of the properties of the aluminium alloy on the blast resistance of FMLs. Particular attention is given to predicting the front and back displacements and the energies dissipated during the blast process. In total, thirty-six cases are studied.

2. Geometric and blast loadings of FML panels

For verification purposes, the FML panels previously subjected to localised blast loading in the experimental study by Langdon et al. ([8]-[10]) are used to validate the current FE models. These 400×400 mm panels (300×300 mm exposed area), were manufactured from sheets of 0.025 in. (approximately 0.6 mm) thick 2024-O aluminium alloy and a woven glass-fibre/polypropylene composite. The FML panels are identified using the notation, AXTYZ-#, as described in (Langdon, 2007a), where A = aluminium, X = number of aluminium layers, T = GFPP, Y = number of blocks of GFPP, Z = number of plies of GFPP per block and # indicates the panel number.

In order to investigate the influence of the properties of the aluminium alloy on the low-impulse blast behavior, FML panels based on the four aluminium alloys, namely

ISBN 978-0-946881-76-5

2012 Wrexham: Glyndŵr University

Table 1
Details of the lay-ups and impulses for verification.

Lay-ups	No. of layers	Thickness (mm)	Impulse (Ns)
A2T18-4	10	5.60	7.94
A3T24-8	11	6.06	7.85
A3T26-3	15	8.10	9.54
A3T28-5	19	9.82	10.34
A4T32-4	10	5.85	7.23
A4T34-5	16	8.73	7.01
A4T36-2	22	11.48	11.61
A4T38-2	28	13.90	11.13
A5T42-4	13	7.46	8.87

2024-O, 2024-T3, 6061-T6 and 7075-T6, subjected to an impulse I = 8 Ns were considered. All four alloys are widely used in the aerospace industry. Details of the lay-ups and impulses investigated in this study are listed in Table 1.

Blast pressure load, calculated from the measured impulse, is a function of both time and distance from the plate centre. The pressure–time history is idealized as a uniform function over a small central region and follows an exponentially decaying function as:

$$P(r,t) = p_1(r)\,p_2(t) \tag{1}$$

where:

$$p_1(r) = \begin{cases} P_0 & r \le r_0 \\ P_0 e^{-k(r-r_0)} & r_0 < r < r_b \\ 0 & r > r_b \end{cases} \qquad p_2(t) = e^{-2t/t_0} \tag{2}$$

where r_0 = 15 mm is the radius of the explosive disc used in the experiments, $r_b < L/2$, L is the length of the panel and t_0 = 0.008 ms is the characteristic decay time for the pulse and k is an exponential decay parameter. The decay parameter is not constant, but a function of the total impulse (Karagiozova et al., 2010). The total impulse is defined as:

Table 2
Johnson-Cook constants for aluminium alloys

Johnson-Cook constants	A (MPa)	B (MPa)	n	C
Al 2024-O (Karagiozova et al., 2010)	85	325	0.40	0.0083
Al 2024-T3 (Lesuer, 2000)	369	684	0.73	0.0083
Al 6061-T6 (Corbett, 2006)	324	114	0.42	0.0020
Al 7075-T6 (Brar et al., 2009)	546	678	0.71	0.0240
Damage constants	D_1	D_2	D_3	D_4
Al 2024-O (Karagiozova et al., 2010)	0.130*	0.130*	-1.500*	0.011*
Al 2024-T3 (Lesuer, 2000)	0.130	0.130	-1.500	0.011
Al 6061-T6 (Corbett, 2006)	-0.770	1.450	-0.470	0.000
Al 7075-T6 (Brar et al., 2009)	-0.068	0.451	-0.952	0.036

* Damage constants for Al 2024-T3 were used due to the lack of available data.

$$I = 2\pi \int_0^{\infty} \int_0^{r_b} P(r,t)\,dr\,dt \tag{3}$$

A user subroutine VDLOAD was used to model the pressure distribution over the exposed area of the plate.

3. Material modelling

3.1 Aluminium layers

The aluminium alloy was modelled as an elasto-plastic material, exhibiting rate-dependent behaviour. Temperature effects in the aluminium alloy were not taken into account. The Johnson-Cook material model was used in the form:

$$\sigma = \left[A + B(\bar{\varepsilon}_{pl})^n\right]\left[1 + C\ln\left(\frac{\dot{\bar{\varepsilon}}_{pl}}{\dot{\varepsilon}_0}\right)\right] \tag{4}$$

where $\bar{\varepsilon}_{pl}$ is the equivalent plastic strain; $\dot{\bar{\varepsilon}}_{pl}$ and $\dot{\varepsilon}_0$ are the equivalent plastic and reference strain rate and A, B, C and n are material parameters.

Damage in the Johnson-Cook material model is predicted using the following cumulative damage law:

$$D = \sum\left(\frac{\Delta\bar{\varepsilon}_{pl}}{\bar{\varepsilon}_f^{pl}}\right) \tag{5}$$

in which:

$$\bar{\varepsilon}_f^{pl} = \left[D_1 + D_2\exp\left(D_3\sigma^*\right)\right]\left[1 + D_4\ln\left(\frac{\dot{\bar{\varepsilon}}_{pl}}{\dot{\varepsilon}_0}\right)\right] \tag{6}$$

where $\Delta\bar{\varepsilon}_{pl}$ is the increment of equivalent plastic strain during an increment in loading and σ^* is the mean stress normalised by the equivalent stress. The parameters D_1, D_2, D_3, and D_4 are constants. Failure is assumed to occur when D = 1. Hence the current failure strain, $\bar{\varepsilon}_f^{pl}$, and thus the accumulation of damage, D, is a function of the mean stress and the strain rate. The constants in the Johnson-Cook model for the four alluminium alloys used in this study are given in Table 2. The Young's modulus, Poisson's ratio and density of the various aluminium alloys were taken as E = 73.1 GPa, ν = 0.3 and ρ = 2690 kg/m^3, respectively.

3.2 Glass fibre reinforced composite layers

3.2.1 The 3D damage model for the composite material

Given that a woven glass-fibre/polypropylene composite layer is produced by placing fibres in a [0^0/90^0] pattern, the material behaviour within the plane of the laminate is similar in those two directions. There is therefore no need to separate the fibre and resin in order to simulate the overall response of the composite ply. Besides, the material tests carried out in this paper were based on the composite laminates, i.e. no individual tests to address fiber and resin separately. Therefore, Hashin's 3D failure criteria (Hashin, 1080) are sufficient to simulate woven glass-fibre/polypropylene composite layer. The failure functions may be expressed as follows:

Fibre tension $(\sigma_{11} \geq 0)$:

$$F_{\mathrm{f}}^{\mathrm{t}} = \left(\frac{\sigma_{11}}{X_{1t}}\right)^2 + \left(\frac{\sigma_{12}}{S_{12}}\right)^2 + \left(\frac{\sigma_{13}}{S_{13}}\right)^2, d_{ft} = 1$$

Fibre compression $(\sigma_{11} < 0)$:

$$F_{\mathrm{f}}^{\mathrm{c}} = \frac{|\sigma_{11}|}{X_{1c}}, d_{fc} = 1$$

Matrix tension $(\sigma_{22} + \sigma_{33} \geq 0)$:

$$F_{\mathrm{m}}^{\mathrm{t}} = \frac{(\sigma_{22} + \sigma_{33})^2}{X_{2t}^2} + \frac{\sigma_{23}^2 - \sigma_{22}\sigma_{33}}{S_{23}^2} + \frac{\sigma_{12}^2 + \sigma_{13}^2}{S_{12}^2}, d_{mt} = 1 \quad (7)$$

Matrix compression $(\sigma_{22} + \sigma_{33} < 0)$

$$F_{\mathrm{m}}^{\mathrm{c}} = \left[\left(\frac{X_{2c}}{2S_{23}}\right)^2 - 1\right]\frac{(\sigma_{22} + \sigma_{33})}{X_{2c}} + \frac{(\sigma_{22} + \sigma_{33})^2}{4S_{23}^2} + \frac{(\sigma_{23}^2 - \sigma_{22}\sigma_{33})}{S_{23}^2} + \frac{\sigma_{12}^2 + \sigma_{13}^2}{S_{12}^2}, d_{mc} = 1$$

where X_{1t}, X_{1c}, X_{2t}, X_{2c}, S_{12}, S_{13} and S_{23} are the various strength components (Hashin, 1980) and d_{ft}, d_{fc}, d_{mt} and d_{mc} are the damage variables associated with the four failure modes.

The response of the material after damage initiation (which describes the rate of degradation of the material stiffness once the initiation criterion is satisfied) is defined by the following equation:

$$\sigma = C(d) \cdot \varepsilon \quad (8)$$

where $C(d)$ is a 6×6 symmetric damaged matrix, whose non-zero terms can be written as:

$$\begin{aligned}
C_{11} &= (1-d_f)E_1(1-\nu_{23}\nu_{32})\Gamma \\
C_{22} &= (1-d_f)(1-d_m)E_2(1-\nu_{13}\nu_{31})\Gamma \\
C_{33} &= (1-d_f)(1-d_m)E_3(1-\nu_{12}\nu_{21})\Gamma \\
C_{12} &= (1-d_f)(1-d_m)E_1(\nu_{21}+\nu_{31}\nu_{23})\Gamma \\
C_{23} &= (1-d_f)(1-d_m)E_2(\nu_{32}+\nu_{12}\nu_{31})\Gamma \\
C_{13} &= (1-d_f)(1-d_m)E_1(\nu_{31}+\nu_{21}\nu_{32})\Gamma \\
C_{44} &= (1-d_f)(1-s_{mt}d_{mt})(1-s_{mc}d_{mc})G_{12} \\
C_{55} &= (1-d_f)(1-s_{mt}d_{mt})(1-s_{mc}d_{mc})G_{23} \\
C_{66} &= (1-d_f)(1-s_{mt}d_{mt})(1-s_{mc}d_{mc})G_{13}
\end{aligned} \quad (9)$$

where the global fibre and matrix damage variables as well as the constant Γ are also defined as:

$$\begin{aligned}
d_f &= 1-(1-d_{ft})(1-d_{fc}) \\
d_m &= 1-(1-d_{mt})(1-d_{mc}) \\
\Gamma &= \frac{1}{1-\nu_{12}\nu_{21}-\nu_{23}\nu_{32}-\nu_{13}\nu_{31}-2\nu_{21}\nu_{32}\nu_{13}}
\end{aligned} \quad (10)$$

where E_i is the Young's modulus in the i direction, G_{ij} is the shear modulus in the i-j plane and ν_{ij} is the Poisson's ratio for transverse strain in the j-direction, when the stress is applied in the i-direction. The Young's moduli, shear's moduli, Poisson's ratios and strengths of the GFPP are given in Table 3.

The factors s_{mt} and s_{mc} in the definitions of the shear moduli are introduced to control the reduction in shear stiffness caused by tensile and compressive failure in the matrix respectively. The following values are recommended in ABAQUS (2009): $s_{mt} = 0.9$ and $s_{mc} = 0.5$.

3.2.2 Strain-rate effects in the mechanical properties

The effects of strain-rate on the mechanical properties of a composite material are typically modelled using strain-rate dependent functions for both the elastic modulus and the strength. Yen (2002) developed logarithmic functions to account for strain-rate effects in a composite material as follows:

$$\begin{aligned}
\{S_{RT}\} &= \{S_0\}\left(1 + C_1 \ln\frac{\dot{\bar{\varepsilon}}}{\dot{\varepsilon}_0}\right) \\
\{E_{RT}\} &= \{E_0\}\left(1 + C_2 \ln\frac{\dot{\bar{\varepsilon}}}{\dot{\varepsilon}_0}\right)
\end{aligned} \quad (11)$$

where:

$$\begin{aligned}
\{\dot{\bar{\varepsilon}}\} &= \{|\dot{\varepsilon}_1| \quad |\dot{\varepsilon}_2| \quad |\dot{\varepsilon}_1| \quad |\dot{\varepsilon}_2| \quad |\dot{\varepsilon}_{12}| \quad |\dot{\varepsilon}_{13}| \quad |\dot{\varepsilon}_{23}|\}^T \\
\{S_{RT}\} &= \{X_{1t} \quad X_{2t} \quad X_{1c} \quad X_{2c} \quad S_{12} \quad S_{13} \quad S_{23}\}^T \\
\{E_{RT}\} &= \{E_1 \quad E_2 \quad E_3 \quad G_{12} \quad G_{13} \quad G_{23}\}^T
\end{aligned} \quad (12)$$

and the subscript 'RT' refers to the rate-adjusted values, the subscript '0' refers to the static value, $\dot{\varepsilon}_0 = 1\ \mathrm{s}^{-1}$ is the reference strain-rate, $\dot{\bar{\varepsilon}}$ is the effective strain-rate, C_1 and C_2 are the strain-rate constants, respectively.

3.2.3 Implementation of the material model in ABAQUS/Explicit

The material model and failure criteria described in the previous sections were implemented in ABAQUS/Explicit using the VUMAT subroutine. This subroutine is compiled and enables ABAQUS/Explicit to obtain the required information regarding the state of the material and the material mechanical response during each time step, at each integration point of each element. The stresses are computed within the VUMAT subroutine using the given strains and the material stiffness coefficients. Based on these stresses, Hashin's 3D failure criteria outlined in Eq.(7) are calculated, and the elastic

Table 3
Properties of the GFPP layers

Elastic properties	Values	Progressive failure	Values
ρ (kg/m^3)	1800	X_{1t} (MPa)	300
E_1 (GPa)	13.0	X_{1c} (MPa)	200
E_2 (GPa)	13.0	X_{2t} (MPa)	300
E_3 (GPa)	2.40	X_{2c} (MPa)	200
G_{12} (GPa)	1.72	S_{12} (MPa)	140
G_{13} (GPa)	1.72	S_{13} (MPa)	140
G_{23} (GPa)	1.69	S_{23}(MPa)	140
ν_{12}	0.1		
ν_{13}	0.3		
ν_{23}	0.3		

modulus and strength values are adjusted for strain-rate effects using Eq.. When an element fails, as determined by the failure criteria, the element status is then changed from 1 to 0. At this point, the stresses at that material point are reduced to zero and it no longer contributes to the model stiffness. When all of the material status points of an element have been reduced to zero, the element is removed from the mesh.

3.3 Cohesive elements and material properties

Debonding at the interface between the composite and aluminium layers was modelled using cohesive elements available in ABAQUS (2009). The elastic response was defined in terms of a traction-separation law with uncoupled behaviour between the normal and shear components. The default choice of the constitutive thickness for modelling the response, in terms of traction versus separation, is 1.0, regardless of the actual thickness of the cohesive layer. Thus, the diagonal terms in the elasticity matrix and density should be calculated using the true thickness of the cohesive layer as follows:

$$K_{nn} = \frac{E_n}{t_c}$$
$$K_{ss} = \frac{E_s}{t_c} \qquad (13)$$
$$K_{tt} = \frac{E_t}{t_c}$$
$$\rho = \rho_c t_c$$

The quadratic nominal stress and energy criterion were used to model damage initiation and damage evolution, respectively. Damage initiated when a quadratic interaction function, involving the nominal stress ratios, reached unity. Damage evolution was defined based on the energy conjunction with a linear softening law. The mechanical properties of the cohesive elements were obtained from Karagiozova et al. (2010) and are given in Table 4.

4. Finite element modelling

The 3D FML panel consisted of the aluminium alloy, the composite and the cohesive layers as three separate parts.

Table 4
Properties of the cohesive layers with thickness 1mm.

Elastic properties			
ρ_c (kg/m^3)	E_n (GPa)	E_s (GPa)	E_t (GPa)
920	2.05	0.72	0.72
Damage initiation			
t_n^0 (MPa)	t_s^0 (MPa)	t_t^0 (MPa)	
140	300	300	
Damage evolution			
G_n^c (J/m^2)	G_s^c (J/m^2)	G_t^c (J/m^2)	
2000	3000	3000	

G_n^c, G_s^c and G_t^c are the critical fracture energies in the normal, the first, and the second shear directions.
t_n^0, t_s^0 and t_t^0 are the critical nominal normal stress, the first and the second shear stresses.

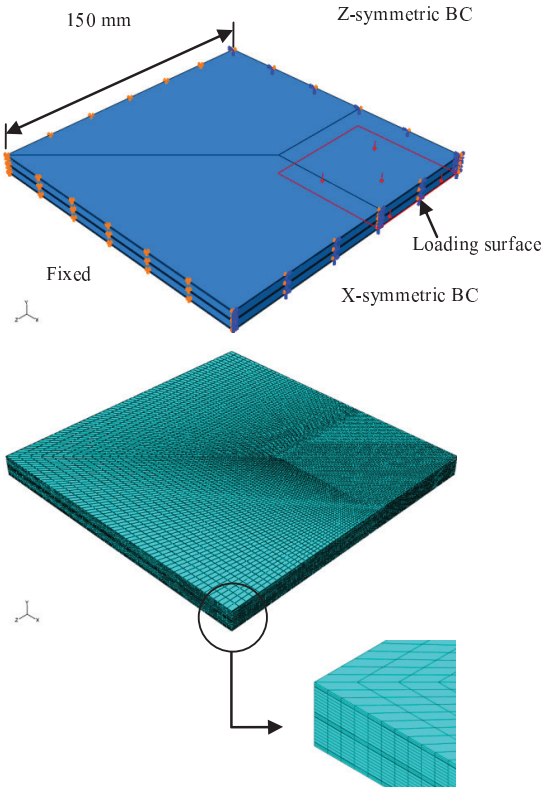

Figure 1. Dimensions, loading, boundary conditions and mesh generation for typical 3/2 FML panel.

The aluminium and composite layers were meshed using C3D8R elements, which are eight-noded, linear hexahedral elements with reduced integration and hourglass control. The individual aluminium and composite plies were discretized with two elements through the thickness. The interfaces between the aluminium and the composite layers were created using eight-node 3D cohesive elements (COH3D8). As the structure has symmetry in both the directions, only a quarter of each FML panel was modeled with the appropriate boundary conditions applied along the planes of symmetry, as shown in Fig. 1. A mesh size of 1×1 mm for a central area of 60×60 mm (Fig. 1) was found to be the most appropriate for these FML panels. Symmetric boundary conditions were applied to the nodes lying on the XY and YZ planes, while the other two edges were fully fixed. The general contact algorithm was used

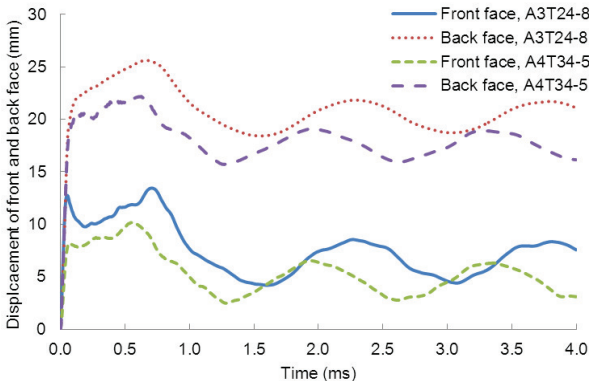

Figure 2. Back and front face displacements versus time for panels A3T24-8 and A4T34-5.

Table 5
Comparison of experimental data from Lemanski et al. (2007) and numerical simulation results of displacements of front and back faces for verification (mm).

Panel	Impulse (Ns)	Experiment		ABAQUS	
		Front	Back	Front	Back
A2T18-4	7.94	4.95	22.19	9.10	16.30
A3T24-8	7.85	6.06	20.34	10.10	19.30
A3T26-3	9.54	4.32	20.35	7.20	23.70
A3T28-5	10.34	3.23	22.59	2.20	20.90
A4T32-4	7.23	9.72	21.73	13.80	17.20
A4T34-5	7.01	4.57	17.48	7.60	14.00
A4T36-2	11.61	1.55	27.21	5.40	22.60
A4T38-2	11.13	1.29	24.59	4.30	20.70
A5T42-4	8.87	7.95	25.31	11.50	19.90

for the definition of contact between the two neighbouring layers of the aluminium and the composite. Surface-based tie constraints were imposed between either the aluminium or the composite layer and the cohesive layer to model adhesion between the adjacent layers.

5. Results and Discussion

Since there are no experimental data available in the literature to describe strain-rate effects in the woven glass-fibre/polypropylene composite, rate-dependent material models, with different values of the strain-rate constant, were investigated in this study. A material model incorporating strain-rate effects in the strength, shear and the through-thickness modulus values was chosen. Strain-rate constant values that agreed well with the experimental results were $C_1 = C_2 = 0.35$. This material model is consistent with results of McCarthy et al. (2004) and Gama and Gillespie (2011). Initially, two FML panels, A3T24-8 and A4T34-5, were studied to investigate their transient and residual displacements. After conducting a number of convergence studies, numerical simulations were carried

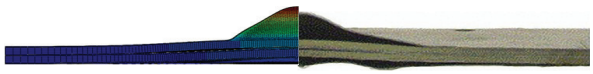

a) A3T28-5, I = 10.34 Ns

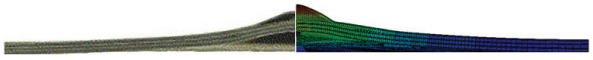

b) A4T32-4, I = 7.23 Ns

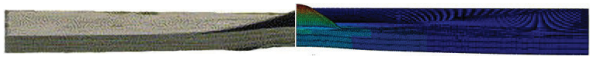

c) A4T34-5, I = 7.01 Ns

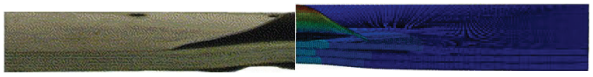

d) A4T36-2, I = 11.61 Ns

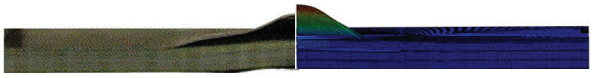

e) A4T38-2, I = 11.13 Ns

Figure 3. Comparison between the experiments and numerical simulations for five FML panels.

Table 6
Summary of permanent front and back face displacements of FMLs based on the four aluminium alloys.

Panel	Aluminium types	Dimensional parameters		
		Impulse (Ns)	Displacement (mm)	
			Front	Back
A2T18	Al 2024-O	8.00	5.53	22.92
	Al 2024-T3	8.00	5.17	18.19
	Al 6061-T6	8.00	5.71	20.84
	Al 7075-T6	8.00	4.50	15.20
A3T24	Al 2024-O	8.00	6.63	18.77
	Al 2024-T3	8.00	7.10	16.29
	Al 6061-T6	8.00	7.20	18.10
	Al 7075-T6	8.00	5.56	12.07
A3T26	Al 2024-O	8.00	4.58	16.21
	Al 2024-T3	8.00	4.42	13.15
	Al 6061-T6	8.00	4.21	15.13
	Al 7075-T6	8.00	2.91	9.30
A3T28	Al 2024-O	8.00	3.28	17.99
	Al 2024-T3	8.00	2.41	12.09
	Al 6061-T6	8.00	2.81	14.80
	Al 7075-T6	8.00	1.20	9.74
A4T32	Al 2024-O	8.00	9.48	24.29
	Al 2024-T3	8.00	8.52	16.42
	Al 6061-T6	8.00	8.04	19.12
	Al 7075-T6	8.00	4.91	12.57
A4T34	Al 2024-O	8.00	4.95	20.42
	Al 2024-T3	8.00	3.02	13.75
	Al 6061-T6	8.00	3.43	15.87
	Al 7075-T6	8.00	1.88	10.82
A4T36	Al 2024-O	8.00	2.36	18.41
	Al 2024-T3	8.00	1.21	13.49
	Al 6061-T6	8.00	1.45	15.64
	Al 7075-T6	8.00	0.47	10.44
A4T38	Al 2024-O	8.00	1.18	17.88
	Al 2024-T3	8.00	0.68	12.92
	Al 6061-T6	8.00	0.71	14.12
	Al 7075-T6	8.00	0.28	10.30

out over a time period of 4 ms. The transient displacement relates to the first peak in the displacement time trace and the residual displacement is taken as the average after more than three cycles following unloading. The variation of the front and back displacements with time are shown in Fig. 2. As expected, the deflections of the thinner A3T24 panel are greater than those of its stiffer A4T34 counterpart. It is worth noting that the difference between the front and back surface displacements is greater than the initial thickness of the panel. This increase in the effective thickness of the FML is associated with the opening up of planes of delamination within the volume of the laminate. FE models of other types of FML panels sub-

jected to a low impulse were also developed to broaden the validation. The experimental and numerical results are presented in Table 5. Reasonable agreement between the predicted and experimental mid-point displacements is observed. Comparing the experimental and numerical failure modes of five typical panels, as shown in Fig. 3, the simulations accurately capture the primary failure mechanisms in the FMLs, which include large out-of-plane plastic displacements, debonding of the back face and local buckling of the internal aluminium layer.

The numerical results corresponding to FML panels based on the four aluminium alloys are presented in Table 6. It can be seen that the front and back displacements of those panels based on the aluminium 7075-T6 are the smallest, whereas those based on the aluminium 2024-O are the largest. This suggests that the properties of the aluminium alloy, most particularly its yield stress, greatly influence the blast response of these hybrid materials. It can be seen that the permanent displacements tend to decrease with increasing yield strength of the aluminium alloy.

6. Conclusions

A parametric study of the low-impulse blast behaviour of FMLs based on different aluminium alloys is presented. Here, three dimensional finite element models of FML panels based on a 2024-O aluminium alloy and a woven glass-fibre/polypropylene composite subjected to low-impulse localised blast loading are developed and validated against previously-published experimental data. Hashin's 3D failure criteria, incorporating strain-rate effects in the GFPP is implemented into ABAQUS/Explicit. Using the validated models, a parametric study is used to investigate the influence of the properties of the aluminium alloy on the blast resistance of FMLs based on the four aluminium alloys, namely 2024-O, 2024-T3, 6061-T6 and 7075-T6. The residual back displacement of the FML panels decreases with the increasing yield strength of the aluminium alloy.

References

ABAQUS (2009). *Theory Manual*, Version 6.9, Hibbitt, Karlsson and Sorensen.

Brar, N.S., Joshi, V.S. and Harris, B.W. (2009). Constitutive model constants for Al7075-T651 and Al7075-T6. In: *Proceedings of AIP Conference*, Vol. 1195, No 1, pp. 945-948.

Compston, P., Cantwell, W.J., Jones, C. and Jones, N. (2001). Impact perforation resistance and fracture mechanisms of a thermoplastic based fiber-metal laminate. *Journal of Materials Science Letters*, Vol. 20, pp. 597-599.

Corbett, B. (2006). Numerical simulations of target hole diameters for hypervelocity impacts into elevated and room temperature bumpers. *International Journal of Impact Engineering*, Vol. 33, No 1-12, pp. 431-440.

Fleisher, H.J. (1996). Design and explosive testing of a blast resistant luggage container. In: *International Conference on Structures under Shock and Impact*, pp. 51-60.

Gama, B.A. and Gillespie, J.W., Jr. (2011). Finite element modelling of impact, damage evolution and penetration of thick-section composites. *International Journal of Impact Engineering*, Vol. 38, No 4, pp. 181-197.

Hashin, Z. (1980). Failure criteria for unidirectional fiber composites, *Journal of Applied Mechanics*, Vol. 47, pp. 329-334.

Karagiozova, D., Nurick G.N. and Langdon, G.S. (2009). Behaviour of sandwich panels subject to intense air blasts – Part 2: Numerical simulation. *Composite Structures*, Vol. 91, No 4, pp. 442-450.

Karagiozova, D., Langdon, G.S., Nurick, G.N. and Yuen, S.C.K. (2010). Simulation of the response of fibre-metal laminates to localised blast loading. *International Journal of Impact Engineering*, Vol. 37, No 6, pp. 766-782.

Kingery, C.N. and Bulmash, G. (1984). *Air Blast Parameters from TNT Spherical Air Burst and Hemispherical Surface Burst*, ARBRL-TR-02555. Aberdeen, ML: Ballistic Research Laboratories.

Kotzakolios, T., Vlachos, D. and Kostopoulos, V. (2011a). Investigation of blast response of GLARE laminates: comparison against experimental results. *Plastics, Rubber and Composites*, Vol. 40, No 6-7, pp. 349-355.

Kotzakolios, T., Vlachos, D. and Kostopoulos, V. (2011b). Blast response of metal composite laminate fuselage structures using finite element modelling. *Composite Structures*, Vol. 93, No 2, pp. 665-681.

Krishnakumar, S. (1994). Fibre metal laminates-the synthesis of metals and composites. *Materials and Manufacturing Processes*, Vol. 9, No 2, pp. 295-354.

Langdon, G.S., Lemanski, S.L., Nurick, G.N., Simmons, M.C., Cantwell, W.J. and Schleyer, G.K. (2007a). Behaviour of fibre-metal laminates subjected to localised blast loading: Part I–Experimental observations. *International Journal of Impact Engineering*, Vol. 34, No 7, pp. 1202-1222.

Langdon, G.S., Nurick, G.N., Lemanski, S.L., Simmons, M.C., Cantwell, W.J. and Schleyer,G.K. (2007b). Failure characterisation of blast-loaded fibre-metal laminate panels based on aluminium and glass-fibre reinforced polypropylene. *Composites Science and Technology*, Vol. 67, No 7-8, pp. 1385-1405.

Langdon, G.S., Cantwell, W.J. and Nurick, G.N. (2007c). Localised blast loading of fibre-metal laminates with a polyamide matrix. *Composites Part B: Engineering*, Vol. 38, No 7-8, pp. 902-913.

Langdon, G.S., Chi, Y., Nurick, G.N. and Haupt, P. (2009). Response of GLARE© panels to blast loading, *Engineering Structures*, Vol. 31, No 12, pp. 3116-3120.

Langdon, G.S., Cantwell, W.J. and Nurick, G.N. (2005a). The blast response of novel thermoplastic-based fibre-metal laminates – some preliminary results and observations. Composites Science and Technology, Vol. 65, No 6, pp. 861-872.

Langdon, G.S., Yuen, S.C.K. and Nurick, G.N. (2005b). Experimental and numerical studies on the response of quadrangular stiffened plates. Part II: localised blast loading. International Journal of Impact Engineering, Vol. 31, No 1, pp. 85-111.

Lemanski, S.L., Nurick, G.N., Langdon, G.S., Simmons, M.C., Cantwell, W.J. and Schleyer, G.K. (2007). Behaviour of fibre metal laminates subjected to localised blast loading–Part II: Quantitative analysis. *International Journal of Impact Engineering*, Vol. 34, No 7, pp. 1223-1245.

Lesuer, D.R. (2000). *Experimental Investigations of Material Models for Ti-6Al-4V Titanium and 2024-T3 Aluminum*, Livermore, CA: Lawrence Livermore National Laboratory.

McCarthy, M.A., Xiao, J.R., Petrinic, N., Kamoulakos, A. and Melito, V. (2004). Modelling of bird strike on an aircraft wing leading edge made from fibre metal laminates–Part 1: Material modelling. *Applied Composite Materials*, Vol. 11, pp. 295-315.

Reyes-Villanueva, G. and Cantwell, W.J. (2004). The high velocity impact response of composite and FML-reinforced sandwich structures. *Composites Science and Technology*, Vol. 64, No 1, pp. 35-54.

Reyes, G. and Cantwell, W.J. (2000). The mechanical properties of fibre-metal laminates based on glass fibre reinforced polypropylene. *Composites Science and Technology*, Vol. 60, No 7, pp. 1085-1094.

Soutis, C., Mohamed, G. and Hodzic, A. (2011). Modelling the structural response of glare panels to blast load. *Composite Structures*, Vol. 94, No 1, pp. 267-276.

Vlot, A. (1996). Impact loading on fibre metal laminates. *International Journal of Impact Engineering*, Vol. 18, No 3, pp. 291-307.

Vogelesang, L.B. and Vlot, A. (2000). Development of fibre metal laminates for advanced aerospace structures. *Journal of Materials Processing Technology*, Vol. 103, No 1, pp. 1-5.

Yen, C.F. (2002). Ballistic impact modeling of composite materials. In: *Proceedings of the 7th International LS-DYNA Users Conference*, Vol. 6, pp. 15-23.